Current Topics in Electrochemistry
Vol. 23, 2021

Original Article

Differentiating metal-support interactions on Pt/C and Pt/C-TiO_2 electrocatalysts

E. Y. Cervantes-Aspeitia[1,2], M. L. Hernández-Pichardo[1,*], R. G. González-Huerta[2] and P. del Angel[3]

[1]Instituto Politécnico Nacional, ESIQIE, Laboratorio de Nanomateriales Sustentables, UPALM, 07738, México City; [2]Instituto Politécnico Nacional, ESIQIE, Laboratorio de Electroquímica y Corrosión, UPALM, 07738 México City; [3]Instituto Mexicano del Petróleo, Dirección de Investigación y Posgrado, Eje Central L. Cárdenas 152, 07730, México City, México.

ABSTRACT

Carbon-TiO_2 composites were prepared by the sol-gel method using different TiO_2 contents (0, 3, 5, and 10 % wt.). Platinum nanoparticles (NPs) were photo-deposited on carbon and carbon-TiO_2 substrates. The catalysts were characterized by X-ray diffraction (XRD), X-Ray photoelectron spectrometry (XPS), high-resolution transmission electron microscopy (HRTEM), and high-angle annular dark-field scanning transmission electron microscopy (HAADF-STEM), and to check the electrocatalytic behavior of the electrodes, the oxygen reduction reaction (ORR) was studied. Photogenerated electrons were used to reduce the platinum cations, and along with a small TiO_2 content, enhance the kinetics of the ORR through an increase of the electron transfer from platinum to the oxygen molecule. However, different phenomena were developed on the surface, depending on the titanium oxide content. The results show the so-called metal-oxide interactions and their effects on electrocatalytic activity.

KEYWORDS: TiO_2, carbon, Pt, photogenerated electrons, SMSI, ORR.

1. INTRODUCTION

Energy electrochemical devices, such as fuel cells, have attracted considerable attention due to their ability to convert energy with high efficiency and without the production of polluting by-products [1-3]. Polymer electrolyte membrane fuel cells (PEMFC) are presently the most suitable devices for mobile and stationary power applications [2, 4]. Nevertheless, durability, sluggish kinetics, and high overpotentials associated with the performance of the catalyst are the most critical issues to be solved in these systems [5]. Oxygen reduction reaction (ORR) is of utmost importance in these technologies; however, the ORR kinetics is still slow due to the difficulties in oxygen adsorption on the electrode surface, O-O bond activation/cleavage, and oxide removal [6, 7]. Up to now, platinum supported on carbon is the best catalyst for the ORR reaction. However, these solids have some disadvantages, such as the high price of platinum and poor stability against carbon corrosion, especially in the cathode where the catalyst works at low pH and high potential and temperatures. These severe conditions lead to the corrosion of carbon and the detachment of metal nanoparticles and, consequently, to the loss of the electrocatalytic activity [4]. Then, the development of robust support is a crucial factor for the commercialization of fuel cell systems. One approach to solving these challenges is to use modified carbon materials using metal oxides such as WO_3, TiO_2, SnO_2, or ZnO [8-10]. Among these oxides, titanium dioxide (TiO_2) has gained considerable attention in fuel cell applications due to its stability in acidic and oxidative

*Corresponding author: mhernandezp@ipn.mx

environments, promoting excellent corrosion resistance [11-18]. Besides, TiO_2 properties might modify the so-called strong metal-support interaction (SMSI) and, hence, the electrocatalytic behavior of TiO_2-supported catalysts [5, 11]. Recently, the group of Professor Vante has proved that it is possible to reduce the amounts of the catalyst when platinum atoms interact with titanium oxide for the ORR in catalysts prepared by photo-deposit [11, 13]. Also, Bukka *et al*. showed that reducing the size of the Pt particles by using this method is another approach for increasing the available active sites for ORR [18]. However, a direct comparison of the catalytic activity of platinum on both supports, Pt/C and Pt/C-TiO_2, at different TiO_2 contents is needed. Thus, in this work, we synthesized a series of Pt/C and Pt/C-TiO_2 catalysts by the photo-deposit process to evaluate the geometric and electronic effects of the electrocatalytic activity of these samples on the ORR.

2. MATERIALS AND METHODS

A series of Pt/C and Pt/C-TiO_2 was prepared by a procedure similar to that reported in [11]. The synthesis was carried out using titanium (IV) butoxide (Aldrich, 97%), Vulcan carbon XC-72 (treated in nitrogen at 400 °C for 4 h), and hexachloroplatinic (IV) acid hydrate (Aldrich, ~38% Pt basis).

2.1. C-TiO_2 composites preparation by the sol-gel method

The C-TiO_2 composites were prepared by the sol-gel method using different TiO_2 contents (3, 5, and 10 % wt.). First, carbon was ultrasonically dispersed in isopropanol for 2 h at room temperature. Then titanium butoxide was added, and the suspension was mixed for 1 h. After this time, the hydrolysis was carried out by the addition of 1 mL of water. The suspension was maintained under continuous stirring for another 24 h at room temperature, and finally, it was washed and dried at 110 °C by 16 h.

2.2. Synthesis of Pt/C and Pt/C-TiO_2 catalysts by photo-deposit

Pt/C and Pt/C-TiO_2 catalysts were prepared with a platinum loading of 10% wt. by photo-deposit. A suspension containing the adequate quantities of the substrate (carbon or carbon-TiO_2), hexachloroplatinic acid, and methanol as a hole scavenger was treated in a photo-reactor (Prendo Q-500) under illumination with a UV lamp (Xe lamp, 250 W) for 3 h. The catalysts were labeled as *PtC* (Pt/C), *PtCT3* (Pt/C-3% wt. TiO_2), *PtCT5* (Pt/C-5% wt. TiO_2), and *PtCT10* (Pt/C-10% wt. TiO_2).

2.3. Electrochemical measurements

The electrocatalytic behavior of the electrodes prepared with the Pt/C and Pt/C-TiO_2 catalysts was studied for the oxygen reduction reaction (ORR) using a conventional single three-electrode test electrochemical cell. The electrode potentials in this work are related to a normal hydrogen electrode (NHE) in a 0.5 M H_2SO_4 aqueous solution electrolyte. The electrochemical measurements were carried out at room temperature using a Potentiostat AUTOLAB. The working electrode was a glassy carbon disk with a 5 mm diameter (0.196 cm^2). The counter electrode was a platinum mesh, and the reference electrode was a normal hydrogen electrode (NHE). The catalytic ink was prepared by dispersing 5 mg of catalyst in 70 μL of Nafion®, 500 μL of water, and 500 μL of N, N-Dimethylformamide in an ultrasonic bath for 2 h. A drop containing 10 μL of catalyst ink was deposited onto the working electrode surface and dried at atmospheric conditions. The Pt loading on the glassy carbon was 16.9, 21.9, 15.6, and 16.3 μg for PtC, PtCT3, PtCT5, and PtCT10. The electrodes were activated in N_2-saturated electrolyte by scanning the potential in a region between 1.2 V/NHE to 0.0 V/NHE at 100 mV/s for 35 cycles until a steady-state voltamperogram was reached. Finally, two cycles were performed at 50 mV s^{-1} in the same potential range to analyze the oxide-reducing signals on the catalyst surface. After that, the electrolyte was saturated with pure O_2 for 10 min and maintained on the electrolyte surface during the rotating disk electrode (RDE) experiments. Hydrodynamic experiments were recorded in the range of rotation rate from 100 to 1600 rpm at 5 mVs^{-1}. The current density was normalized for a geometric area of 0.196 cm^2.

2.4. Physicochemical characterization

The catalysts were characterized by X-ray diffraction (XRD), high-resolution transmission

electron microscopy (HRTEM), scanning transmission electron microscopy (STEM), and X-ray photoelectron spectroscopy (XPS). The XRD analyses were carried out by using a diffractometer RIGAKU model Miniflex 600 with an X-ray tube with Cu radiation Kα (λ = 1.5418 Å). The used power was 40 kV and 15 mA with a step of 0.02 and a speed of 5°/min. The XPS spectra were obtained in K-Alpha equipment from Thermo Scientific, which has an Al Kα source and a monochromator. The general spectra were obtained by using step energy of 160 and 60 eV for the high-resolution spectra. In the case of these samples, a load compensation system was used.

HRTEM and STEM analyses were obtained with a JEOL JEM2200FS microscope, operated at 200 kV, and equipped with a Cs probe corrector. In this instrument, HRTEM and high angle annular dark field (HAADF-STEM) images were obtained using a CCD camera and Digital Software from Gatan. The elemental composition was determined by Energy Dispersive X-ray Spectroscopy (EDS) with a Noran spectrometer fitted to the TEM. The powder samples were ultrasonically dispersed in ethanol and supported on a holey carbon-coated copper TEM grid.

3. RESULTS AND DISCUSSION

3.1. Electrochemical assessment of Pt/C and Pt/C-TiO_2 catalysts

The PtC, PtCT3, PtCT5, and PtCT10 electrocatalysts with 0, 3, 5, and 10% wt. of TiO_2, respectively, were studied for the oxygen reduction reaction. RDE measurements were carried out to evaluate the kinetic parameters of the ORR. The polarization curves of the different catalysts are given in Figure 1.

The onset potential was found to be around 0.97 V, and from the Tafel plots, the Tafel slope was found to be 84, 72, 74, and 79 mV dec^{-1} for PtC, PtCT3, PtCT5, and PtCT10, respectively. These values indicated a mechanism where the first electron transfer rate Tafel is the determining step.

The PtCT3 electrode showed higher diffusion limiting current than Pt/C. It was considered that increases in the limiting current are associated with the rise of oxygen diffusion through the electrode surface. Then, a positive effect on the reduction process of the incorporation of TiO_2 to the carbon substrate at 3% is observed. Moreover, in the inset of Figure 1, the cyclic voltammetry characterization of the electrodes prepared with

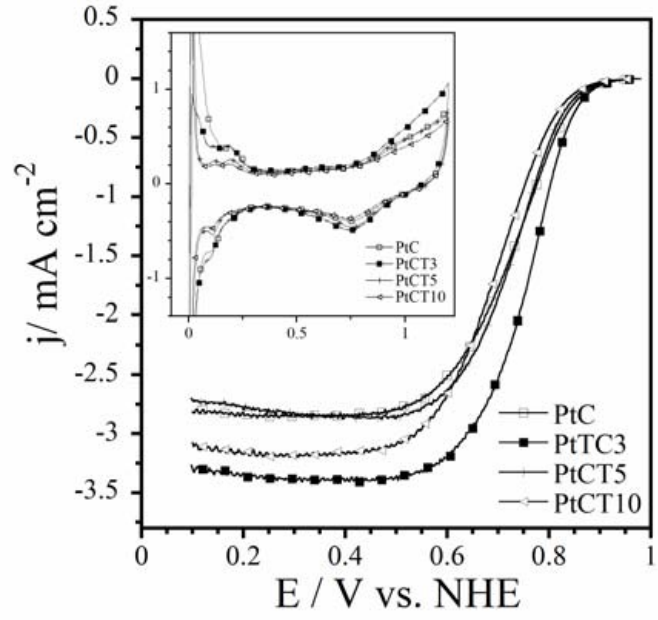

Figure 1. Polarization curves of the Pt/C, PtCT3, PtCT5, and PtCT10 catalysts at a rotating speed of 1600 rpm at 25 °C in 0.5 M H_2SO_4 in O_2-saturated electrolyte. Inset: Cyclic voltammetry of the electrocatalyst in a 0.5 M H_2SO_4 solution.

these samples is shown. These electrodes present adsorption-desorption hydrogen region (H_{upd}) in a potential region of about 0.1 to 0.3 V/NHE, which is characteristic of polycrystalline noble metals. However, all the electrodes present different characteristics depending on the catalyst composition. It is observed that the electrodes prepared with the catalysts prepared with TiO_2 present different signals in the H_{upd} region than the blank PtC electrode. These peaks are not well defined on the Pt/C-TiO_2 samples. The cathodic scan shows the signals corresponding to the reduction of the oxides formed during the anodic sweep. The reduction peaks show a slight displacement to a positive potential according to the decrease in the TiO_2 content. On the other hand, the PtCT10 catalyst shows a remarkable difference in the current magnitude in all potential scans. This electrode presents a low electrochemically active area in the hydrogen region as well as low oxygen reduction activity. It could be the result of the TiO_2 migration on the Pt surface, covering the active sites generating geometrical effects, as we explain below [19].

3.2. Physicochemical characterization

3.2.1. X-ray diffraction patterns (XRD)

X-ray diffraction patterns for the Pt/C and Pt/C-TiO_2 samples are shown in Figure 2. It shows the characteristics peaks of the Vulcan XC-72R carbon in 25° (002) and 43° (101) two-theta, indicating that the carbon is a polycrystalline material.

The presence of the TiO_2 phase in anatase form was identified; the diffraction peaks appear like small shoulders, which means that crystallites of TiO_2 of size around 4 nm were formed. Small diffraction peaks in 2θ have the position of about 36.9°, 37.8°, 48°, 53.8°, 55°, and 62.5°, that refer to the (103), (004), (200), (105), (211), and (204) planes of TiO_2, respectively in the anatase form (JCPDS 00-021-1272) [11]. Interestingly, there are no XRD peaks for platinum metal, indicating that the particles are lower than 4 nm, which is the detection limit of the instrument.

3.2.2. Transmisssion electron microscopy (TEM) and scanning transmission electron microscopy (STEM)

TEM bright-field images of the PTCT3 catalyst

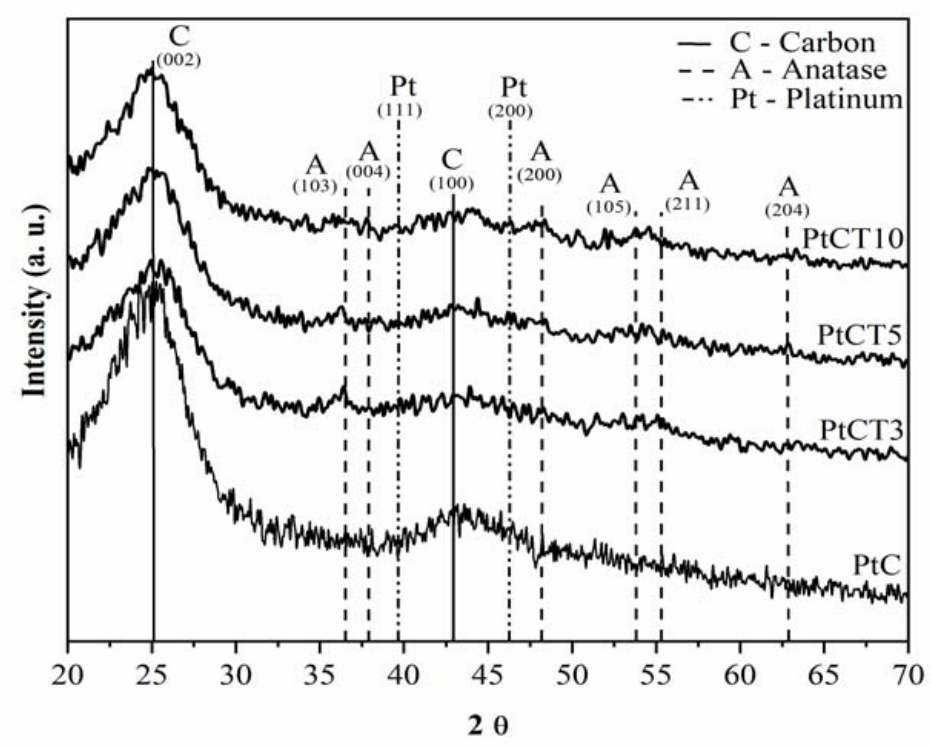

Figure 2. XRD patterns for Pt/C and Pt/C-TiO_2 catalysts.

(Figure 3a, b) show the morphology of the sample. The Pt and the TiO_2 NPs are homogeneously dispersed on carbon Vulcan; this is deduced from the EDS obtained in this region (Figure 3c). The Ti, O, Pt, and C were detected. The Cu and Fe peaks in the spectrum correspond to the holder of the microscope.

HAADF-STEM is an advanced tool that could provide comprehensive information about the formation of the Pt nanoparticles over C-TiO_2. Figure 3d shows a HAADF-STEM image of intermediate magnification of the PTCT3 catalyst, where different contrast between the Pt nanoparticles and the support can be observed. This sample has 3% wt. of TiO_2 and 10% wt. of Pt, and this means that Pt is much higher in content than Ti. In this case, the nanoparticles observed in HAADF-STEM images correspond to Pt. Figure 3e and f show the same region at higher magnification; Pt nanoparticles between 1 and 2.5 nm in size are observed, which is in accord with XRD results. Additionally, the particle size of the Vulcan carbon presents sizes from 30 to 60 nm, with an onion-like morphology. This is important because many Pt nanoparticles are in the edges of these particles of Vulcan carbon, as is observed bottom left in Figure 3e. Other regions have the same characteristics.

These results are in good agreement with prior works that have reported that the use of photochemical methods allows the formation of ultra-small platinum NPs size [11, 18]. A photocatalytic behavior in certain materials of carbon treated under UV irradiation has been observed, even in the absence of semiconductors [20]. Then, the spillover of these photoelectrons onto the conducting carbon is possible. These electrons reduce the platinum salt precursor and generate Pt NPs on carbon or carbon-TiO_2 substrates. As these photogenerated electrons are available all over the substrates, there will be numerous nucleation sites to form ultra-small NPs [18]. However, the photoirradiation of UV-light of H_2PtCl_6 in a water-ethanol solution also leads to the reduction of Pt^{4+} to Pt^0 [12].

The small size of the Pt NPs can be explained due to the creation of photogenerated electrons during the photo-depositing process. This movement of electrons, especially on the support, generates numerous nucleation to form smaller Pt NPs. It is interesting to note that the photoreduction of Pt was also carried out in the catalyst without TiO_2 (PtC). In the literature, it has been reported that H_2PtCl_6 is reduced by UV irradiation [12]; however, a photocatalytic behavior was also found in certain carbon materials treated under UV irradiation in the absence of semiconductors [20].

The absorption of light has been found to lead to the formation of electron/hole pairs on the surface. Therefore, the reduction of platinum can be carried out in the presence of methanol as a sacrificial agent [21].

$$CH_3OH + h^+ \rightarrow {}^{\bullet}CH_2OH + H^+ \quad (1)$$

$${}^{\bullet}CH_2OH \rightarrow CH_2O + H^+ + e^- \quad (2)$$

These results may explain the higher activity of the samples with low content of TiO_2 in the ORR since the amount of electron density transferred to the metal is found critically and inversely proportional to the size of the metal clusters [14]. On the other hand, it is well known that in the TiO_2 anatase phase, the electrons can move faster than in another phase due to the indirect bandgap that enables excited electrons to be stabilized themselves at a lower level in the conduction band leading to higher mobility [13]. Thus, reducing the particle size by this synthesis method and the incorporation of low contents of TiO_2 is a suitable approach for increasing the number of active sites for ORR.

3.2.3. XPS

Finally, XPS analyses were carried out to investigate the chemical composition and surface binding states of the Pt/C and Pt/C-TiO_2 catalysts. High-resolution spectra in the Pt 4f region are shown in Figure 4.

The high-resolution spectra of Pt 4f could be fitted into three doublets associated with their different oxidation states. The most intense doublet, around 70.9 and 74.1 eV, was attributed to metallic Pt. The second one at about 71.8 and 76.2 eV could be assigned to oxidized Pt, probably in the form of platinum oxides. And the third pair of peaks around 79.0 eV and 81.4 eV correspond well with the signals for Pt^{4+} [15].

The above is an indication that the photoreduction process was not enough to reduce all platinum to the zero-valent state. Table 1 shows that the

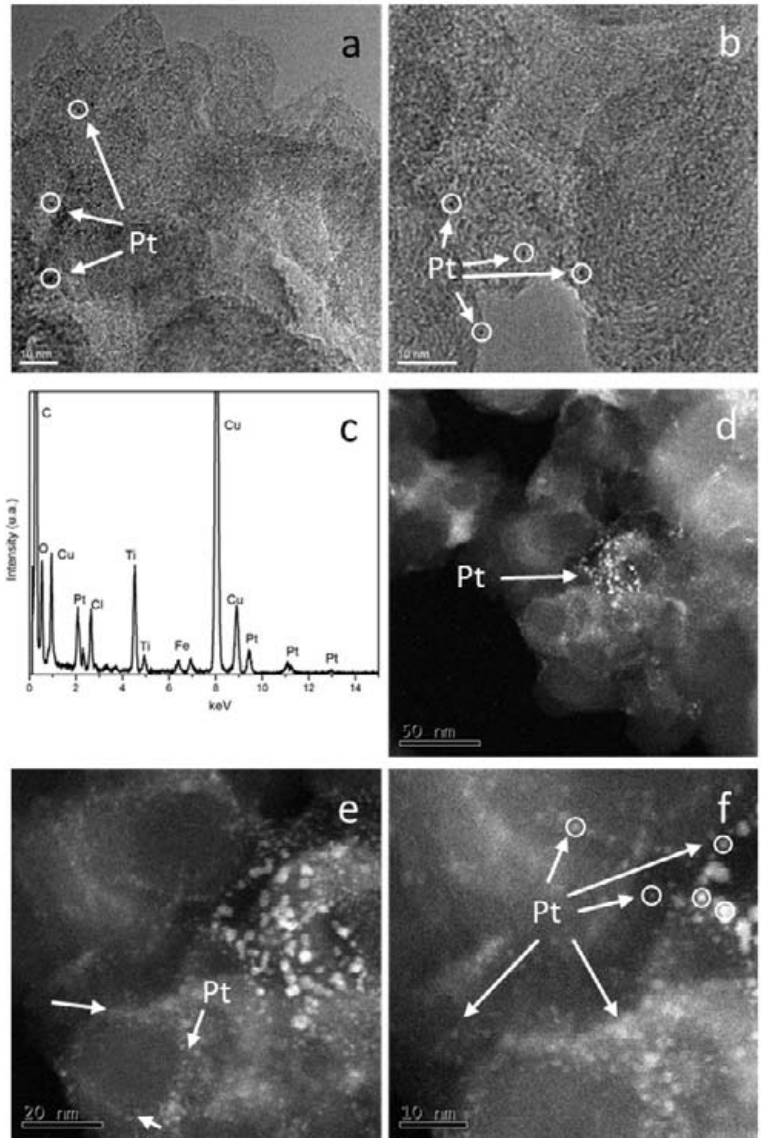

Figure 3. a) and **b)** TEM bright-field images of the PtCT3 sample: the Pt NPs and TiO_2 are not clearly distinguished; **c)** EDS analysis indicating the presence of Pt, Ti, O, and C; **d)**, **e)** and **f)** Z contrast images: the distribution of Pt on the C-TiO_2 support is observed.

samples prepared with TiO_2 present a higher percentage of reduction to metallic platinum due to the photocatalytic activity of this oxide. However, it is observed that as the titania content is increased, this percentage decreases, probably due to a screening effect. This phenomenon results in a reduction of the photonic efficiency of the process. It is produced when the TiO_2 concentration is high, which prevents the surface of the catalyst from being illuminated [22]. This result is indicative of the geometric effect in Pt/C-TiO_2 catalysts in SMSI state [19], in which the migration of the TiO_x species from the reduced support onto the metal catalysts could block the active sites for ORR.

For the catalyst without TiO_2 (Pt/C), the signals of Pt $4f_{7/2}$ and Pt $4f_{5/2}$ were identified at 71.9 and 75.2 eV, respectively. These signals for the samples with TiO_2 were found between 72.2 and 72.4 eV for Pt $4f_{7/2}$ and between 75.6 and 75.9 eV for Pt $4f_{5/2}$. This shift towards higher binding energies in the samples prepared with TiO_2 suggests an electronic interaction of Pt with other species in the sample,

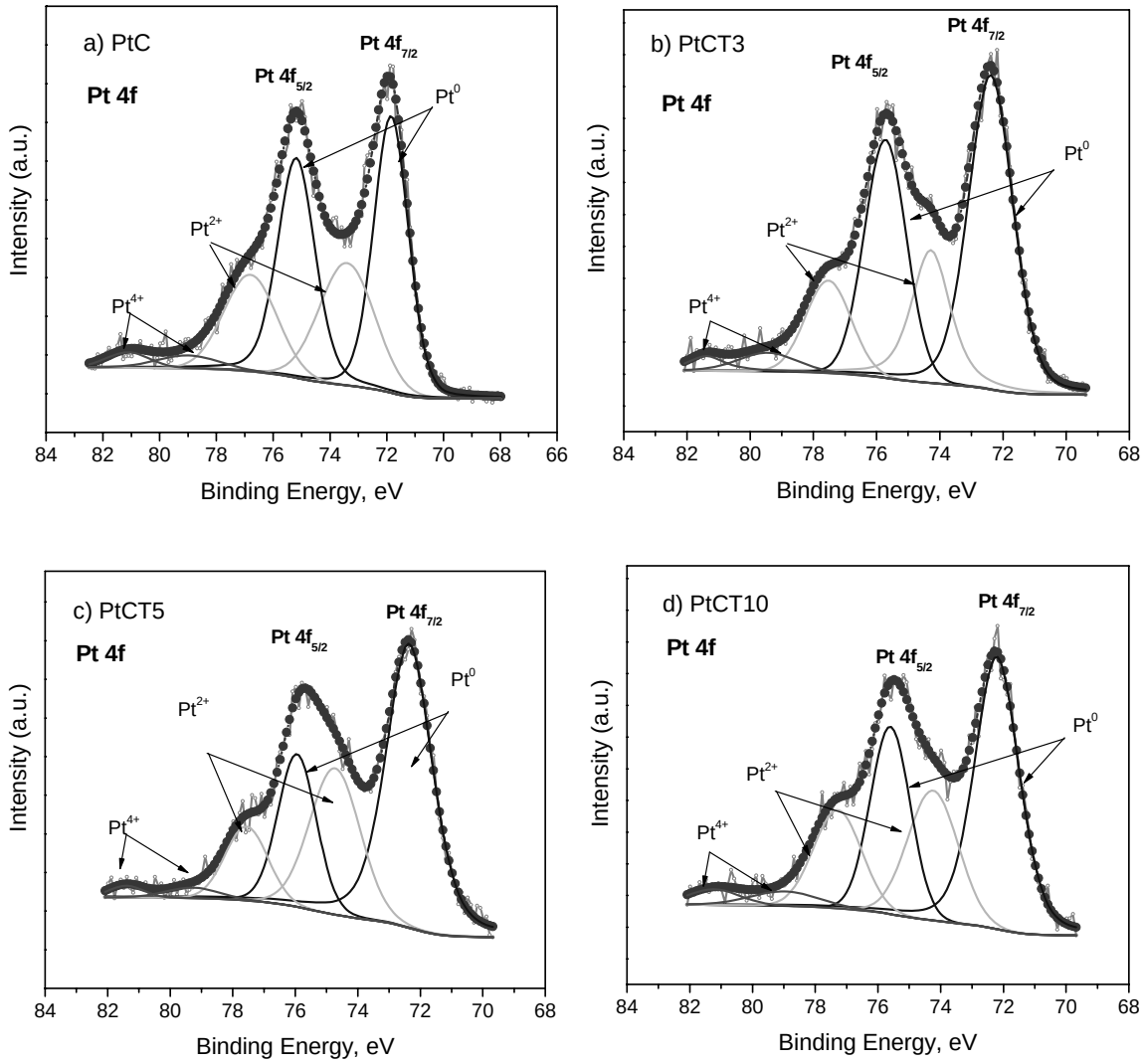

Figure 4. High resolution XPS spectra of the samples: **a**) PtC, **b**) PtCT3, **c**) PtCT5 and **d**) PtCT10 in the Pt 4f region.

in this case, with TiO_2, carbon, and oxygen. It is well known that the ORR is kinetically limited by a slow electron transfer between the catalyst and the adsorbed oxygen. This shift indicates that the availability of electron density on Pt can enhance the interaction with available oxygen in the electrolyte and can ease the electron transfer to the oxygen molecule.

On the other hand, Figure 5 shows the high-resolution spectra in the Ti 2p region for catalysts with different TiO_2 contents. The binding energy of the Ti $2p_{1/2}$ and Ti $2p_{3/2}$ levels are observed at approximately 458.6 and 464.3 eV with ~5.7 eV maximum separation, confirming the status of Ti^{4+} in the TiO_2 anatase phase [16].

The analysis of peaks in the O1s region (Figure 6) provides complementary information to that from the Pt4f and Ti2p spectra. The O1s signal reveals different surface oxygenated species, which strongly depend on the substrate.

It is observed that for Vulcan carbon, only C=O (533.7 eV) and C–O (532.3 eV) signals are observed [23]. When platinum is incorporated, a new peak appears at about 531.4 eV assigned to the platinum-oxygen binding. Finally, the samples prepared with TiO_2 showed a fourth signal at about 530.01 eV associated with the lattice oxygen in the TiO_2 [24]. When the content of TiO_2 is increased, the oxygen related to the Ti-O increases in the surface, due to

Table 1. Fit parameters for Pt 4f photoelectron line.

Catalyst	Chemical State	Area (%)	Binding Energy (eV)	
			Pt $4f_{7/2}$	Pt $4f_{5/2}$
PtC	Pt^0	59.3	71.9	75.2
	Pt^{2+}	36.1	73.4	76.8
	Pt^{4+}	4.6	79.0	81.1
PtCT3	Pt^0	67.3	72.4	75.7
	Pt^{2+}	27.7	74.3	77.5
	Pt^{4+}	5.0	79.5	81.4
PtCT5	Pt^0	64.8	72.4	75.9
	Pt^{2+}	32.3	74.7	77.6
	Pt^{4+}	2.9	79.3	81.4
PtCT10	Pt^0	62.0	72.2	75.6
	Pt^{2+}	32.8	74.3	77.3
	Pt^{4+}	5.2	79.0	81.2

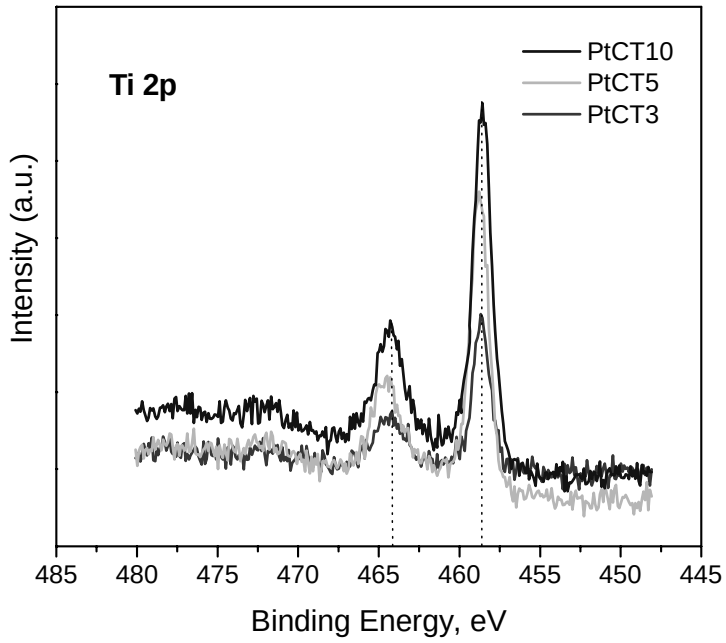

Figure 5. High-resolution XPS spectra of the TiO_2 samples in the Ti 2p region.

the increase in the content, but it also could be due to the covering of Pt NPs by the TiO_x species.

Hence, these results show that the SMSI may modify the electrocatalytic activity of Pt/C-TiO_2 samples on the ORR, depending on the TiO_2 content. A small content (3-5 % wt) may enhance the kinetics of the ORR through an increase of the electron transfer from platinum to the oxygen molecule. On the other hand, a higher content (10 % wt) may modify the electrocatalytic activity of Pt/C-TiO_2 samples on the ORR since it may produce blocking of the active sites for the ORR, generating a decrease of the catalytic activity of Pt/C-TiO_2 samples.

4. CONCLUSIONS

It was found that the synthesis of Pt/C-TiO_2 by the photo-deposit method allows the formation of Pt

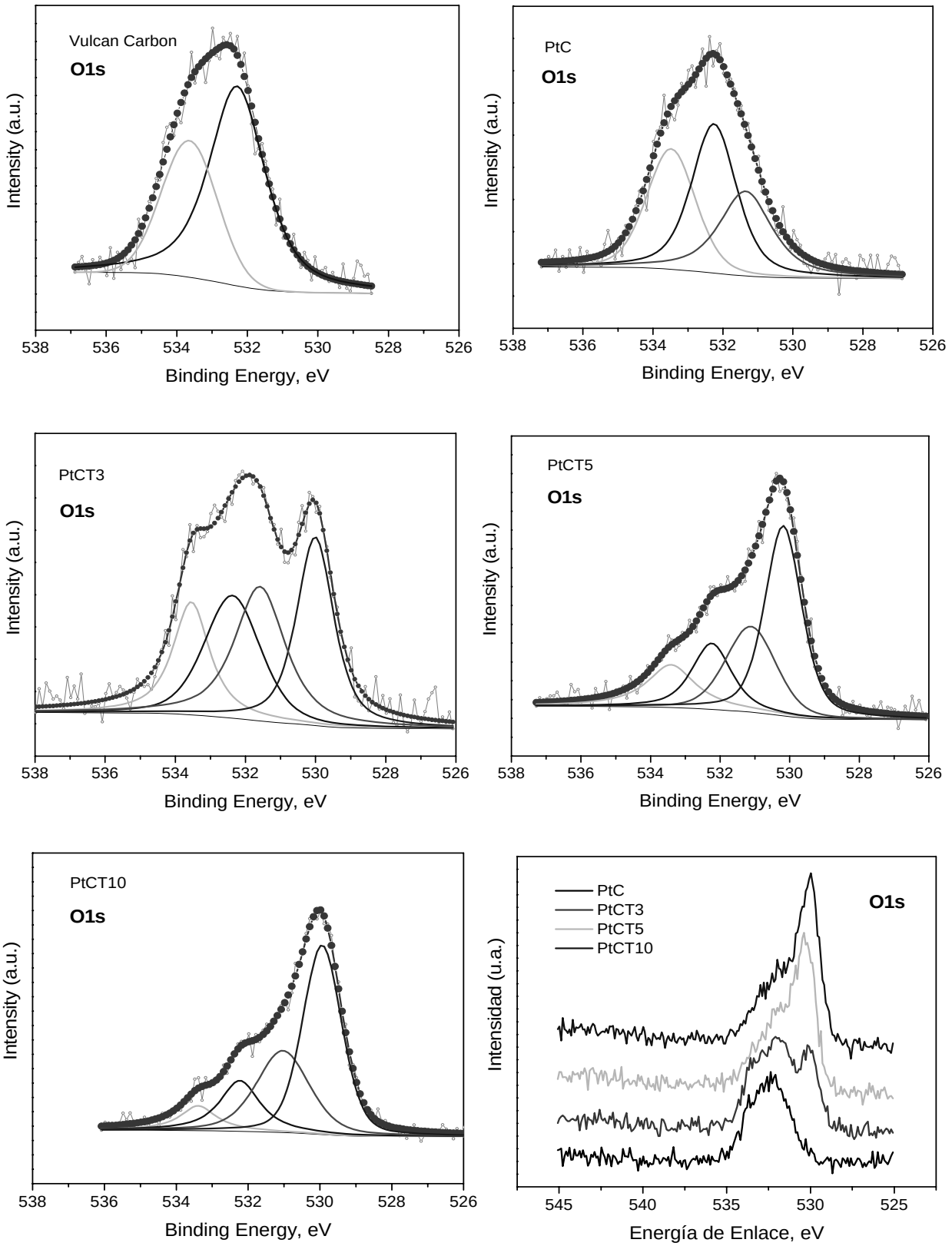

Figure 6. High-resolution XPS spectra of Vulcan carbon, PtC, PTCT3, PTCT5, and PTCT10 catalysts in the O1s region.

NPs smaller than 3 nm, well dispersed on the C-TiO_2 substrate. This work showed that in the synthesis of the Pt/C sample by photo-deposit, the reduction of platinum cations could be carried out by a combined effect of light irradiation and the presence of photogenerated electrons on the carbon surface. This intimate contact of the small Pt NPs with the support allows the SMSI effects. We found that two different interaction mechanisms coexist, an electronic effect involving electron transfer from Pt to TiO_2 and a second one involving a geometric effect. A small TiO_2 content enhances the kinetics of the ORR through an increase of the electron transfer from platinum to the oxygen molecule. Besides, at a higher content, TiO_2 covers the active platinum sites and generates a decrease of the catalytic activity of Pt/C-TiO_2 samples in the ORR by a geometric effect.

ACKNOWLEDGMENTS

This work was supported by the Instituto Politecnico Nacional (Projects SIP-2024 and 20210097) and CONACyT (CB A1-S-15770). EYCA thanks the financial support from CONACyT within the Ph.D. fellowship.

CONFLICT OF INTEREST STATEMENT

The authors declare that they have no conflict of interest.

REFERENCES

1. Takeshita, T. 2012, Green Energy and Technology, Bentham Science Publishers, France.
2. Offer, G. J. 2009, Platin. Met. Rev., 53, 219.
3. Liang, J., Miao, Z., Ma, F., Pan, R., Chen, X., Wang, T., Xie, H. and Li, Q. 2018, Chinese J. Catal., 39, 583.
4. Wang, J., Yin, G., Shao, Y., Zhang, S., Wang, Z. and Gao, Y. 2007, J. Power Sources, 171, 331.
5. Mirshekari, G. R. and Rice, C. A. 2018, J. Power Sources, 396, 606.
6. Nie, Y., Li, L. and Wei, Z. 2015, Chem. Soc. Rev., 44, 2168.
7. Kong, J. and Cheng, W. 2017, Chinese J. Catal., 38, 951.
8. Hernández-Pichardo, M. L., González-Huerta, R. G., del Angel, P., Tufiño-Velazquez, M. and Lartundo, L. 2015, Int. J. Hydrog. Energy, 17371.
9. Ruiz Camacho, B., Morais, C., Valenzuela, M. A. and Alonso-Vante, N. 2013, Catal. Today, 202, 36.
10. Timperman, L., Lewera, A., Vogel, W. and Alonso-vante N. 2010, Electrochem. commun., 12, 1772.
11. Timperman, L., Feng, Y. J., Vogel, W. and Alonso-Vante, N. 2010, Electrochim. Acta, 7558.
12. Ruiz Camacho, B., González Huerta, R. G., Valenzuela, M. A. and Alonso-Vante, N. 2011, Top. Catalysis, 512.
13. Estudillo-Wong, L. A., Luo, Y., Díaz-real, J. A. and Alonso-Vante, N. 2016, Appl. Catal. B, Environm., 187, 291.
14. Badam, R., Vedarajan, R., Okaya, K., Matsutani, K. and Matsumi, N. 2016, Sci. Rep., 6, 1.
15. Wang, M., Wang, Z., Wei, L., Li, J. and Zhao, X. 2017, Chinese J. Catal., 38, 1680.
16. Eckardt, M., Gebauer, C., Jusys, Z., Wassner, M., Hüsing, N. and Behm, R. J. 2018, J. Power Sources, 400, 580.
17. Huynh, T. T., Pham, H. Q., Van Nguyen, A., Bach, L. G. and Ho, V. T. T. 2019, Ind. Eng. Chem. Res., 58, 675.
18. Bukka, S., Badam, R., Vedarajan, R. and Matsumi, N. 2019, Int. J. Hydrog. Energy, 44, 4745.
19. Pan, C., Tsai, M., Su, W. and Rick, J. 2017, J. Taiwan Inst. Chem. Eng., 74, 154.
20. Luo, Y., Heng, Y., Dai, X., Chen, W. and Li, J. 2009, J. Solid State Chem., 182, 2521.
21. Guzman, F., Chuang, S. S. C. and Yang, C. 2013, Ind. Eng. Chem. Res., 52, 61.
22. Fernández-Ibáñez, P., Malato, S. and De Las Nieves, F. J. 1999, Catal. Today, 54, 195.
23. Senthil Kumar, S. M., Soler Herrero, J., Irusta, S. and Scott, K. 2010, J. Electroanal. Chem., 647, 211.
24. Ratova, M., Tosheva, L., Kelly, P. J. and Ohtani, B. 2019, Sustain. Mater. Techno., 22, e00112.